Representation of the Equatorial Undercurrent in CMIP5 Models

LAUREN B. KUNTZ AND DANIEL P. SCHRAG

Department of Earth and Planetary Sciences, Harvard University, Cambridge, Massachusetts

(Manuscript received 12 January 2020, in final form 20 August 2020)

ABSTRACT: The Equatorial Undercurrent (EUC) is a vital component of tropical Pacific circulation, helping to modulate the state of the equatorial Pacific Ocean. Here we compare the representation of the EUC in models from phase 5 of the Coupled Model Intercomparison Project (CMIP5) with observations of the undercurrent. We find that the CMIP5 models consistently underestimate both the magnitude and variability of the EUC. Insufficient resolution as well as diffusivity parameterizations both contribute to a representation of the EUC that is too weak and too diffuse. Given the strong influence of the EUC on the evolution of tropical Pacific sea surface temperatures, model deficiencies in the EUC contribute to shortcomings in capturing ENSO dynamics and Pacific decadal variability. Further evaluation of the impact of EUC simulation on the climatology and variability in the tropical Pacific is necessary.

KEYWORDS: Thermocline circulation; Climate models; Ensembles; Model evaluation/performance; Oceanic variability

1. Introduction

The equatorial Pacific Ocean is a region that is critical to global climate (Kosaka and Xie 2013; England et al. 2014; Fyfe and Gillett 2014; Trenberth et al. 2014). Variability in this region drives variability around the globe (Alexander et al. 2002; Trenberth et al. 2002), making an understanding of the mechanisms that regulate the equatorial Pacific and how they will respond to anthropogenic forcing essential to forecasting future climate changes (Broecker 2017). Global climate models, however, struggle to reproduce the base state of the eastern equatorial Pacific and tropical dynamics (Zhang and McPhaden 2006; Karnauskas et al. 2012; Yang et al. 2014; Wang et al. 2014; Richter 2015; Zuidema et al. 2016; Coats and Karnauskas 2018). The cold tongue in the equatorial Pacific is consistently too cold and reaches too far west in models, even in models that are part of phase 5 of the Coupled Model Intercomparison Project (CMIP5) (Lin 2007; Li et al. 2015; Burls and Fedorov 2014). The oceanic thermocline is often overly diffuse, and models struggle to capture the frequency, spatial footprint, and strength of the El Niño–Southern Oscillation (ENSO) (van Oldenborgh et al. 2005; Guilyardi 2006; Imada and Kimoto 2006; Guilyardi et al. 2012; Bellenger et al. 2014; Zhu and Zhang 2018).

Part of the challenge in modeling equatorial Pacific dynamics stems from the complex interplay of physical processes in both the ocean and atmosphere. Various feedback mechanisms, including the Bjerknes feedback and heat flux feedback, impact the evolution of tropical dynamics (Jin et al. 2006; Guilyardi et al. 2012; Bellenger et al. 2014). The spatial pattern of sea surface temperatures (SSTs), wind stress, and the structure of the thermocline are all coupled on relatively short time scales. For example, a more diffuse thermocline weakens the response of the equatorial Pacific SST to shifts in thermocline depth, subsequently impacting wind feedbacks (Imada and Kimoto 2006; Guilyardi et al. 2012). Likewise, biases in other ocean regions can impact the equatorial Pacific by altering atmospheric teleconnections (Thomas and Fedorov 2017). Improving our understanding of the physical mechanisms that control the tropical Pacific and how those mechanisms are simulated in models is essential to properly capturing equatorial dynamics. Otherwise, apparent improvements in model simulation of the equatorial Pacific may stem from error cancellation, rather than robust advances in physics, providing little validity to model projections (Guilyardi et al. 2012; Bellenger et al. 2014).

The Equatorial Undercurrent (EUC), which supplies cold, nutrient-rich waters to the eastern equatorial Pacific, plays a major role in equatorial dynamics (Bryden and Brady 1985; Karnauskas et al. 2012; Kuntz and Schrag 2018). The EUC interacts with surface waters in the equatorial Pacific through both heat and momentum fluxes, setting the climatological SST gradient (Bjerknes 1966; Coats and Karnauskas 2018).

Karnauskas et al. (2012) studied the simulation of the EUC in the CMIP3 models, finding the velocity to be too slow and diffuse relative to observations. Despite these deficiencies, Karnauskas et al. (2012) noted that net equatorial transports were the proper magnitude, suggesting that this would not bias the mean state. However, the strength of EUC transport impacts variability across time scales. EUC flow rates impact shear stress and instability, potentially influencing mixing and the development of tropical instability waves (TIWs), as well as the thermocline depth and strength; these subsequently impact heat transport and temperature evolution in the surface and subsurface, as well as ENSO dynamics (Sun et al. 1998; Karnauskas et al. 2007, 2008; Moum et al. 2009; Drenkard and Karnauskas 2014; Liu et al. 2016). Properly capturing the magnitude and variability of the EUC is essential to capturing the dynamics of the tropical Pacific. For example,

Supplemental information related to this paper is available at the Journals Online website: https://doi.org/10.1175/JPO-D-20-0007.s1.

Corresponding author: Lauren B. Kuntz, lkuntz2013@gmail.com

DOI: 10.1175/JPO-D-20-0007.1

TABLE 1. List of CMIP5 models investigated in this study.

Model name	Institution	Country
ACCESS1.0 ACCESS1.3	Commonwealth Scientific and Industrial Research Organisation (CSIRO) and Bureau of Meteorology	Australia
CanESM2	Canadian Centre for Climate Modeling and Analysis	Canada
CMCC-CESM CMCC-CM CMCC-CMS	Centro Euro-Mediterraneo per i Cambiamenti Climatici	Italy
CNRM-CM5 CNRM-CM5-2	Centre National de Recherches Météorologiques/Centre Européen de Recherche et Formation Avancée en Calcul Scientifique	France
CSIRO Mk3.6.0 CSIRO Mk3L.1.2	Queensland Climate Change Centre of Excellence and CSIRO	Australia
FGOALS-g2	State Key Laboratory of Numerical Modeling for Atmospheric Sciences and Geophysical Fluid Dynamics (LASG), and Center for Earth System Science (CESS)	China
GFDL CM2.1 GFDL CM3 GFDL-ESM2G GFDL-ESM2M	NOAA/Geophysical Fluid Dynamics Laboratory	United States
GISS-E2-H-CC GISS-E2-H GISS-E2-R-CC GISS-E2-R	NASA Goddard Institute for Space Studies	United States
HadCM3 HadGEM2-CC HadGEM2-ES	Met Office Hadley Centre	United Kingdom
IPSL-CM5A-LR IPSL-CM5A-MR IPSL-CM5B-LR	Institute Pierre Simon Laplace	France
MIROC4h MIROC5 MIROC-ESM-CHEM MIROC-ESM	The University of Tokyo, National Institute for Environmental Studies and Japan Agency for Marine-Earth Science and Technology	Japan
MPI-ESM-LR MPI-ESM-MR MPI-ESM-P	Max Plank Institute for Meteorology	Germany
MRI-CGCM3 MRI-ESM	Meteorological Research Institute	Japan
NorESM1-ME NorESM1-M	Norwegian Climate Centre	Norway

Jochum et al. (2008), explored the role of lateral ocean viscosity on ocean dynamics, finding that reducing viscosity resulted in general improvement in the equatorial circulation, including more realistic EUC core velocities, but also resulted in excessive deepening of the EUC, creating a vertical gradient in the eastern equatorial Pacific that was too gradual (Jochum et al. 2008). Small et al. (2014) used a higher-resolution version of the Community Earth System Model (CESM) (0.1° in the ocean) to explore the global ocean circulation, finding that the equatorial SST gradient in the high-resolution model compared well with observations, but the SST variance was too small (Small et al. 2014); they argued that excessive depth of the thermocline in their simulations might be due to the absence of a spatially dependent diffusivity.

In this paper, we explore how the CMIP5 models simulate the magnitude and variability of the EUC. We compare individual runs from both historical and preindustrial control simulations of models included in the CMIP5 ensemble with observations from the Tropical Atmosphere Ocean (TAO) buoy array. By investigating the differences in model resolution and physics between simulations with the best and poorest EUC representation, we highlight key aspects of the underlying physics that can be used to guide future model improvements.

2. Methods

a. Observational datasets

We use current measurements from the equatorial buoy in the TAO array at 220°E to explore the variability in EUC transport strength (TAO Project Office 2000). Data from other locations in the TAO array are sparse but can be found in the online supplemental material. We primarily use data from acoustic Doppler current profilers (ADCP), which profile the upper 200–300 m at roughly 8-m resolution from roughly 1980 to 2015 (the buoys each have data gaps in this time period). We fill in missing data with information from current meters, which cover the upper 300 m with four–seven discrete

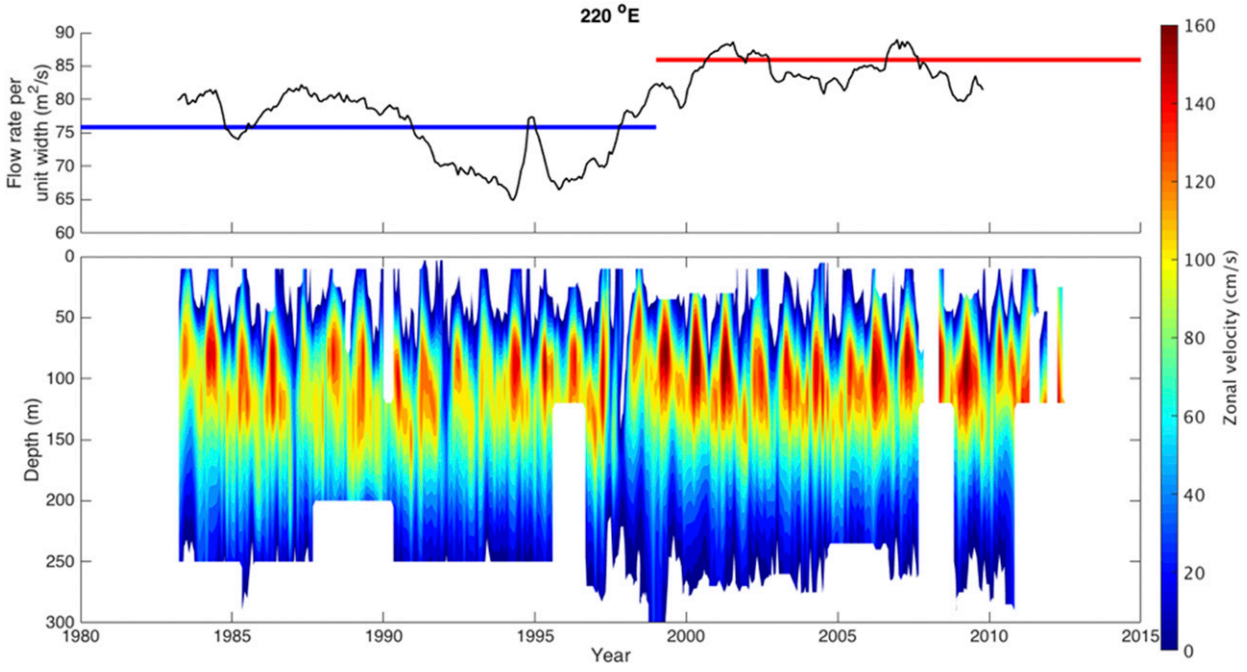

FIG. 1. Zonal velocity along the equator from the TAO buoy at 220°E, using both acoustic Doppler current profilers and current-meter data. To focus on the EUC, only positive (eastward) zonal velocities are shown in the contour plot. An increase in current strength is evident after 1999. The line plot highlights this change, showing average flow rate per unit width above 80 cm s^{-1} before and after 1999, as well as the 5-year running mean (black). The record from the 250°E buoy shows a similar signal (first figure in the online supplemental material), but the records from the other TAO buoys are not complete enough to perform this analysis.

measurements. For reference, at 220°E the core of the EUC is generally between 50 and 150 m. To create a smooth profile and fill in any measurement gaps with depth, we perform a piecewise cubic interpolation on the monthly data, calculating velocity every 5 m. To look at the EUC flux, we define the core of the undercurrent to be the region with velocities greater than 80 cm s^{-1}. We calculate the depth-integrated velocity over that region for months with observations. We discard the fluxes from a given month if the velocity of the bottommost measurement exceeds 80 cm s^{-1}. Because some of the velocity profiles do not cover the full depth range over which zonal velocity is positive, this removes the possibility that the buoy only sampled part of the EUC for that month. Prior to averaging data, we remove the seasonal cycle to avoid biasing the average due to months with missing data. We do not include the 1997/98 El Niño and following La Niña in the calculation of the seasonal cycle.

b. *CMIP5 model data*

We use all preindustrial and historical ensemble members of 37 models from the CMIP5 repository that had oceanic zonal velocity data available at the time of download (Table 1; see the online supplemental material for plots of each individual simulation). The ocean component of these models varies, not only in terms of resolution, but also in terms of physical parameterizations of subgrid-scale processes and vertical coordinates. To compare the model results with observations, we look at the time series of the EUC at 220°E for each individual run in both the historical and preindustrial control simulations. Because the grids differ between models, we interpolate the data spatially to 0°, 220°E for all model runs.

We identify the four models that best capture the magnitude of EUC flux (GFDL CM2, GFDL-ESM2M, HadGEM2-CC, and MIROC4h), as well as the four with the poorest simulation (CSIRO Mk3.6.0, CSIRO Mk3L.1.2, GISS-E2-H, and MPI-ESM-LR), and focus further exploration on these. We calculate the frequency spectrum of maximum velocity at 220°E for these model runs. Because the MPI-ESM-LR model, which struggles to capture the EUC, has a high-resolution version that shows substantial improvement, MPI-ESM-MR, we also compare these two simulations and model configurations.

3. Results

Figure 1 shows observations from the TAO array at 220°E. The core of the EUC lies between 50- and 100-m depth, with peak velocities reaching up to 160 cm s^{-1}. Around 2000, there is a distinct acceleration in the maximum EUC velocities of roughly 20%–25% while the flow rate per unit width in the core of the current rises 10%–15%. As compared with the earlier part of the record, these higher flow rates are sustained. Other records from the TAO buoys show similar changes in the current strength but are less complete (see, e.g., the first few figures in the online supplemental material).

In general, the CMIP5 models simulate an EUC that is too weak and too deep compared to observations. The time series of EUC flow rates at 220°E is shown for the poorest and best

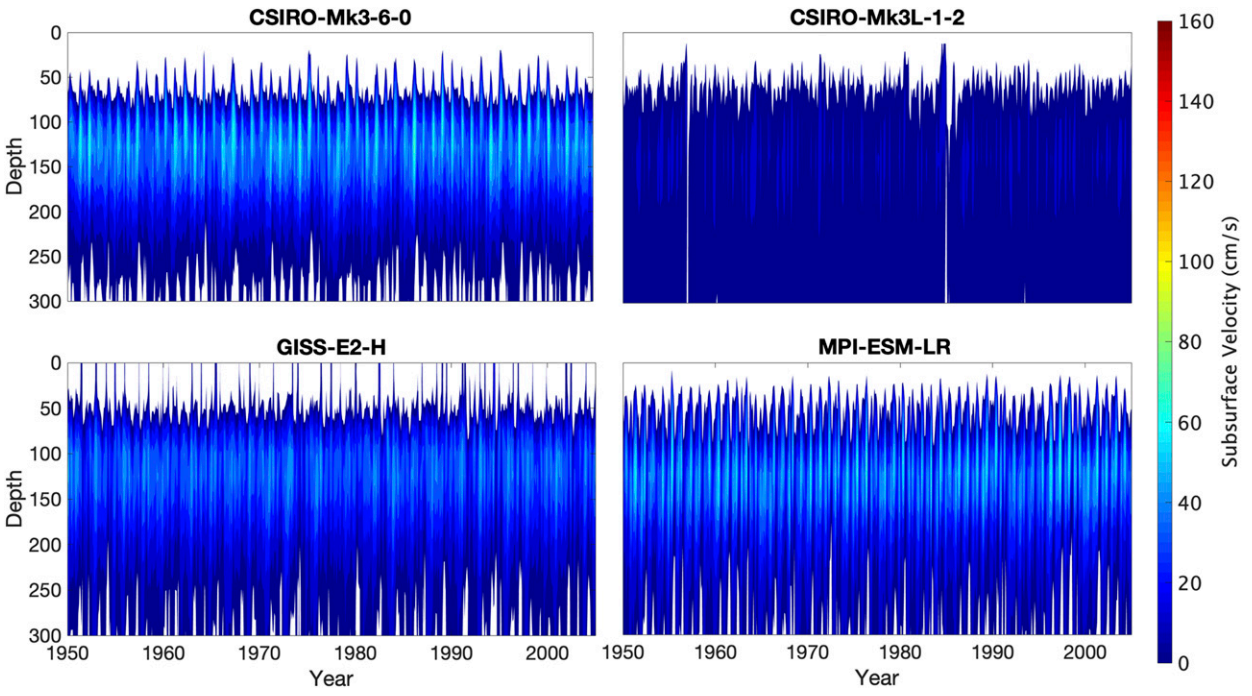

FIG. 2. Time series of the EUC at 220°E from historical runs of the four CMIP5 models with the poorest representation of the EUC. Although the historical runs extend farther back in time, only the period from 1950 to 2005 is shown for consistency with other simulations. The color scale from Fig. 1 is used here for direct comparison.

model simulations in Figs. 2 and 3, respectively (time series for additional runs and other CMIP5 models are included in the online supplemental material). Assessments of best and worst models were done by visual inspection based on comparing the peak EUC velocities and integrated flow rates to observations. Although the worst models clearly stand out, additional best models could have been chosen. Plots for all CMIP5 models can be found in the online supplemental material. The peak velocity of the EUC in the poorest model simulations does not exceed 60 cm s^{-1}. In the best EUC simulations, peak velocities are closer to 120 cm s^{-1} but often still fall short of observations. Table 2 describes differences in these models in terms of mixing schemes, diffusion and viscosity parameterizations, and resolution.

Table 2 also compiles the fidelity of each model's ENSO representation. There is not a clear relationship between EUC and ENSO representation; models with both weak and strong EUCs have ENSO simulations that are too weak or too strong. However, of the models with the best EUC, the GFDL-ESM2M has previously been noted to be the only model of the CMIP5 ensemble to forecast weaker warming in the eastern equatorial Pacific than the west (Kohyama et al. 2017). This model is the exception—the other three models with good representations of the EUC agree with the majority option of an El Niño–like trend in the equatorial Pacific—yet does suggest a deeper understanding of relationships in modeled EUC and ENSO realism is warranted.

Figure 4 shows the time series of the EUC at 220°E for two runs of the MPI-ESM model, one with low resolution (LR) and one with a higher resolution that is eddy resolving (MR). Outside differences in resolution and parameterization of subgrid-scale eddies in LR, the physics in these models is identical (Jungclaus et al. 2013). Although MPI-ESM-LR has one of the weakest EUC simulations, the EUC in MPI-ESM-MR is substantially stronger—actually stronger than observations. The EUC in the higher-resolution case is also shallower, at depths closer to what is seen in the TAO array.

Figure 5 shows the power spectrum of peak EUC velocity at 220°E for both the models with the best and poorest EUC. In general, the models with the stronger EUC flow rates show greater variability across interannual and decadal time scales relative to models with weaker EUC velocities. Of the poor-performing models, GFDL CM2.1 has notably diminished variability at lower frequencies when compared with the others. Power spectra for other runs of these models are similar and are available in the online supplemental material.

This alignment of variability with EUC strength is also seen in the MPI-ESM models (Fig. 6). Although the general shape of the power spectra is similar, the low-resolution model is distinctly lower than the higher-resolution, eddy-resolving model across all interannual and decadal frequencies.

4. Discussion

Like the CMIP3 models (Karnauskas et al. 2012), the CMIP5 models simulate an EUC that is generally too weak and diffuse as compared with observations from the TAO array. As Karnauskas et al. (2012) suggested, resolution plays a role; in general, the models with the best simulation of the EUC have

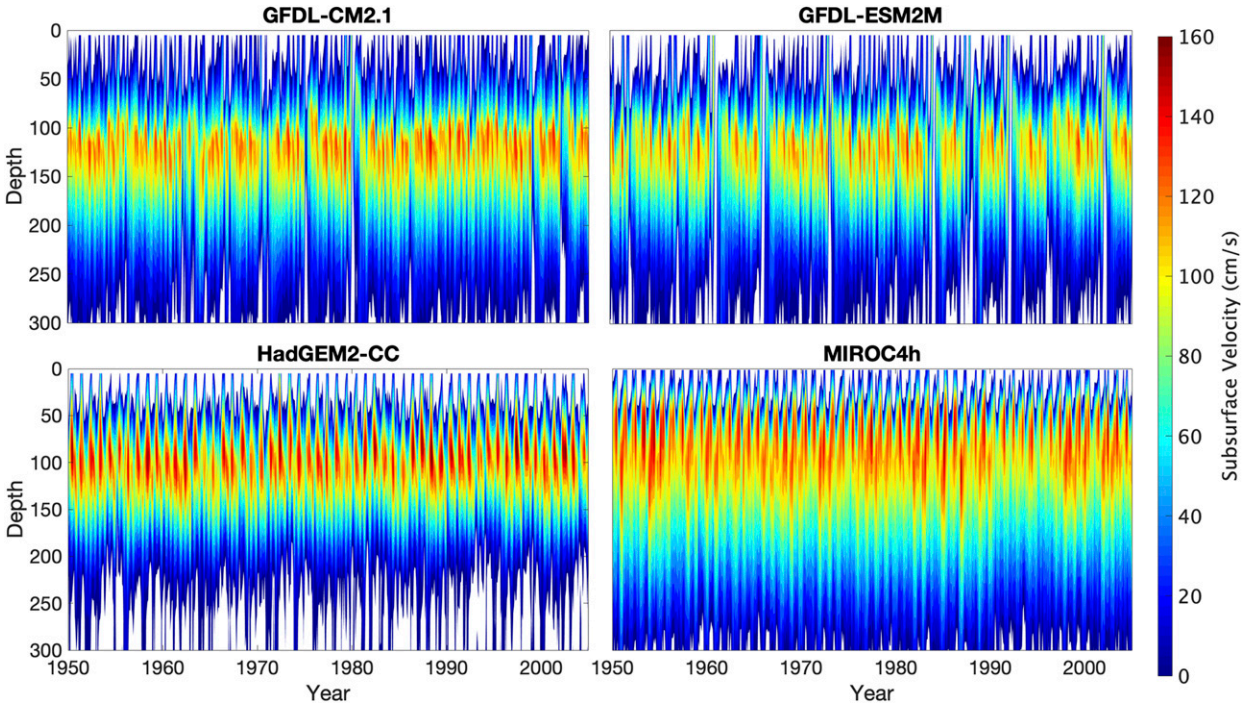

FIG. 3. Time series of the EUC at 220°E from historical runs of the four CMIP5 models with the best representation of the EUC. Although the historical runs extend farther back in time for most runs, only the period from 1950 to 2005 is shown for consistency with the MIROC4h simulation that starts in 1950. The color scale from Fig. 1 is used here for direct comparison.

increased horizontal resolution compared to models with poorer representations of the EUC (Table 2). Three CMIP5 models that have pairs of runs with higher and lower ocean horizontal resolution (CSIRO Mk3L.1.2 and CSIRO Mk3.6.0, MIROC4h and MIROC5, and MPI-ESM-LR and MPI-ESM-MR). The mean velocity of the core of EUC averaged over the model simulation run time are much higher for the model with the higher resolution (~300%). This result is not surprising, as coarser resolution will undoubtedly diminish gradients in any property (Haidvogel and Beckmann 1999). Vertical resolution also tends to be higher in models with the best simulation of the EUC. Given that most models with higher horizontal resolution also have higher vertical resolution, it is not clear how large of an impact vertical grid spacing has on the EUC simulation. Although the MPI-ESM-LR and MPI-ESM-MR have the same vertical grid and physics (excluding eddy fluxes), the EUC in the higher horizontal resolution model is significantly stronger than the low-resolution model. This suggests that vertical resolution is not the sole control on EUC simulation; when there are enough vertical layers in the upper part of the ocean, other factors exert a stronger control on the magnitude of the simulated EUC. There is also a hint that atmospheric resolution may also affect the EUC in these models. Two versions of the IPSL model have identical ocean resolution but different atmospheric resolution; the higher atmospheric resolution also had a slightly higher core EUC velocity, although by only 9.3%.

Roberts et al. (2009) specifically cited diffusivity parameterizations as contributing to weakened EUC flow rates. While high-resolution models are able to use biharmonic dissipation, low-resolution models need to use both Laplacian and biharmonic dissipation to widen unresolved currents and reduce noise. This distinction inherently improves the simulation of tropical dynamics in high-resolution models, yet as Roberts et al. (2009) demonstrated, changing the dissipation parameterizations can reverse these resolution dependent distinctions. Including Laplacian dissipation in a high-resolution model degraded the simulation of the tropical Pacific to the low-resolution case, while removing Laplacian dissipation in a low-resolution model improved the representation of the tropical Pacific (but also decreased model stability) (Roberts et al. 2009). Two of three non-eddy-resolving models in the group of CMIP5 models with the best EUC include spatially varying viscosities that take advantage of the impacts of tropical dissipation parameterizations. The HadGEM2-CC model specifically includes spatially varying viscosity, with reduced background vertical viscosity in the thermocline and horizontal viscosity in the tropics, to improve the simulation of the EUC without increased resolution (Martin et al. 2011). This strategy was cited by Small et al. (2014) as a reason why their high-resolution CESM runs did not simulate the equatorial Pacific very well (Small et al. 2014), with an excessive deepening of the thermocline in the east. The GFDL-ESM2M model also decreases the background vertical diffusivity in the tropics (Dunne et al. 2012). Thus, it appears that a combination of both resolution and dissipation parameterizations contributes to overall EUC simulation. This is consistent with Jochum et al. (2008), who found that decreasing viscosity increased EUC

TABLE 2. Description of CMIP5 models with the best and poorest representation of the EUC. The four CMIP5 models with the best representation of the EUC are in boldface type. The MPI-ESM-MR, IPSL-CM5A-LR, and IPSL-CM5A-MR models are neither the best nor worst models but are included for comparison across models with versions varying in resolution.

Model	EUC representation	Atmosphere equatorial resolution	Ocean equatorial resolution	Vertical layers (no. of layers in top 300 m)	Vertical mixing/diffusivity	Eddy parameterization	ENSO representation	References
CSIRO Mk3.6.0	EUC too weak	~1.9° × 1.9°	~1° × 1.9°	30 layers; z (13)	Spatially varying Visbeck et al. (1997) scheme; Kraus and Turner (1967) mixed layer parameterization	Spatially varying Visbeck et al. (1997) scheme	ENSO is too strong and too slow	Collier et al. (2011); Gordon et al. (2010)
CSIRO Mk3L.1.2	EUC too weak	~3° × 5.6°	~3° × 5.6°	21 layers; z (8)	Vertical diffusivity proportional to N^{-1}	Gent and McWilliams (1990) scheme	ENSO too weak and too slow	Phipps et al. (2011)
GISS-E2-H	EUC too weak	2° × 2.5°	cos(lat) × 1°	26 layers; hybrid z–ρ (12)	Diapycnal coefficient proportional to N^{-1} below mixed layer	Dependent on grid size and total deformation (Smagorinsky 1963)	ENSO is too strong and too frequent	Schmidt et al. (2014); Sun and Bleck (2006)
MPI-ESM-LR	EUC too weak	~1.9° × 1.9°	~1.5° × 1.5°	40 layers; z (15)	Vertical diffusivity based on Richardson no.	Gent et al. (1995) scheme	ENSO too strong but frequency well represented	Jungclaus et al. (2013)
GFDL CM2.1	EUC max velocity and flux comparable to observations; EUC core too deep; not enough decadal variability	2° × 2.5°	~1/3° × 1°	50 layers; z (28)	K-profile parameterization (Large et al. 1994)	Gent and McWilliams (1990) scheme	ENSO is too strong and too frequent	Griffies et al. (2011, 2005)
GFDL-ESM2M	EUC max velocity and flux slightly less than observations; EUC core too deep; not enough decadal variability	2° × 2.5°	~1/3° × 1°	50 layers; z (28)	K-profile parameterization (Large et al. 1994); background diffusivity decreases at equator	Gent and McWilliams (1990) scheme	ENSO is too strong and too frequent	Dunne et al. (2012)
HadGEM2-CC	EUC max velocity and flux comparable to observations; not enough decadal variability	1.25° × 1.875°	~1/3° × 1°	40 layers; z (20)	Vertical diffusivity based on Richardson no. (Peters et al. 1988); reduced vertical diffusivity in the thermocline	Spatially varying Visbeck et al. (1997) scheme; reduced viscosity in tropics	ENSO too weak and too sharply peaked at 6–7 yr	Martin et al. (2011); Johns et al. (2006)
MIROC4h	EUC max velocity and flux slightly greater than observations	~0.56° × 0.56°	~0.1875° × 0.28°	47 layers; hybrid z–ρ (20)	Noh and Kim (1999) scheme	Eddy permitting	ENSO too weak and too sharply peaked at 4 yr	Sakamoto et al. (2012)

TABLE 2. (*Continued*)

Model	EUC representation	Atmosphere equatorial resolution	Ocean equatorial resolution	Vertical layers (no. of layers in top 300 m)	Vertical mixing/diffusivity	Eddy parameterization	ENSO representation	References
MPI-ESM-MR	EUC too strong; not enough decadal variability	~1.9° × 1.9°	~0.4° × 0.4°	40 layers; z (15)	Vertical diffusivity based on Richardson no.	Eddy permitting	ENSO too strong but frequency well represented	Jungclaus et al. (2013)
IPSL-CM5A-LR	EUC too weak; not enough decadal variability	1.875° × 3.75°	~0.5° × 2°	31 layers; z (19)	Diapycnal mixing proportional to N^{-1}	Gent and McWilliams (1990) scheme	ENSO strength well represented but too frequent	Dufresne et al. (2013); Mignot et al. (2013)
IPSL-CM5A-MR	EUC too weak; not enough decadal variability	1.25° × 2.5°	~0.5° × 2°	31 layers; z (19)	Diapycnal mixing proportional to N^{-1}	Gent and McWilliams (1990) scheme	ENSO strength well represented but too frequent	Dufresne et al. (2013); Mignot et al. (2013)

core velocities closer to observations but resulted in a deepening of the EUC that introduced other problems, particularly in the eastern equatorial Pacific (Jochum et al. 2008).

Resolution and dissipation may also explain the disparity in interannual and decadal variability between the CMIP5 models with well represented and poorly represented EUCs. Increased horizontal ocean resolution tends to decrease base-state biases; and proper simulation of long-term climatology is necessary to realistically simulate short-term variability (Dawson et al. 2013). Higher resolutions are also able to capture smaller scale effects, which add variability. For instance eddy-resolving models are able to simulate TIWs, which impact mixing and heat and momentum budgets, and could be important for regulating the equatorial Pacific (Sun et al. 1998; Jochum and Murtugudde 2006; Menkes et al. 2006; Moum et al. 2009; Brown et al. 2010; Liu et al. 2016). The EUC also impacts these fluxes, contributing to shear induced mixing and instabilities that can promote TIWs. This suggests the proper spectrum of EUC variability is necessary to capture the proper spectrum of variability in the surface of the Pacific. For instance, ENSO variability shows an association with TIW activity, with El Niño events linked to suppression of TIWs (Yu and Liu 2003); as the EUC strength also modulates TIW probability, the absence of this physics in models could contribute with the poor representation of ENSO dynamics in the CMIP5 ensemble (Guilyardi et al. 2012; Bellenger et al. 2014).

The TAO observational record is too short to fully describe the spectrum of decadal and multidecadal variability and therefore to compare with decadal variability in the CMIP5 models. However, previous studies have shown that CMIP5 models capture the pattern of Pacific decadal variability but not necessarily the frequency nor the magnitude of SST variability (e.g., Sheffield et al. 2013; Lyu et al. 2016). One possible explanation for this is that a weaker and more diffuse EUC in many CMIP5 models compared with observations may result in weaker SST variance in the eastern equatorial Pacific, and therefore will tend to underrepresent decadal and multidecadal variability. It has been suggested that deficiencies in the mean state contribute to these deficiencies in variability (Lyu et al. 2016), but it is also possible that models fail to capture some of the physics of internal variability in the ocean. Additional effort should be placed on understanding sources of decadal and multidecadal variability in both the EUC and Pacific basin, as well as how they are represented in models.

5. Conclusions

An analysis of the representation of the Equatorial Undercurrent (EUC) in CMIP5 models, and comparison with observations from the TAO array, shows that, with very few exceptions, the CMIP5 models simulate the EUC with a core velocity weaker than observations and with smaller than observed variability, particularly on decadal time scales. Most of these models can still reproduce the base state of transport and heat flux as long as they accurately simulate the net flux of the EUC (Karnauskas et al. 2012); however, properly simulating peak flow rates in the EUC is necessary for

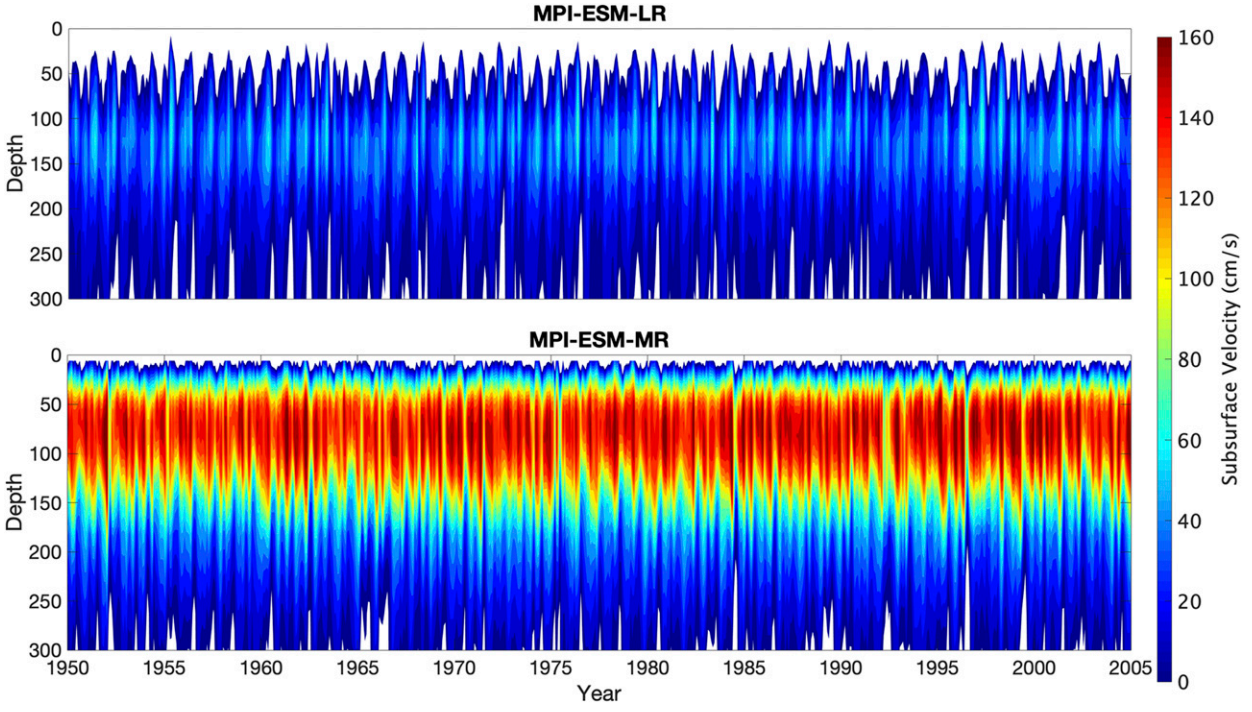

FIG. 4. Time series of the EUC at 220°E from historical runs of MPI-ESM at a low-resolution (LR) and mixed-resolution (MR) grid. With the exception of the grid resolution, and the parameterizations of eddies resolved in MR that are not resolved in LR, the model physics is identical. The color scale from Fig. 1 is used here for direct comparison.

reproducing shear induced mixing, instabilities, and various modes of variability. Given that the core velocity of the EUC is strongly correlated with eastern equatorial Pacific SSTs, the representation of the EUC directly influences the evolution of tropical SSTs on multiple time scales. The exact implications of these model deficiencies on the climatology and variability in the tropical Pacific requires additional analysis, but a better EUC (both in terms of core velocity

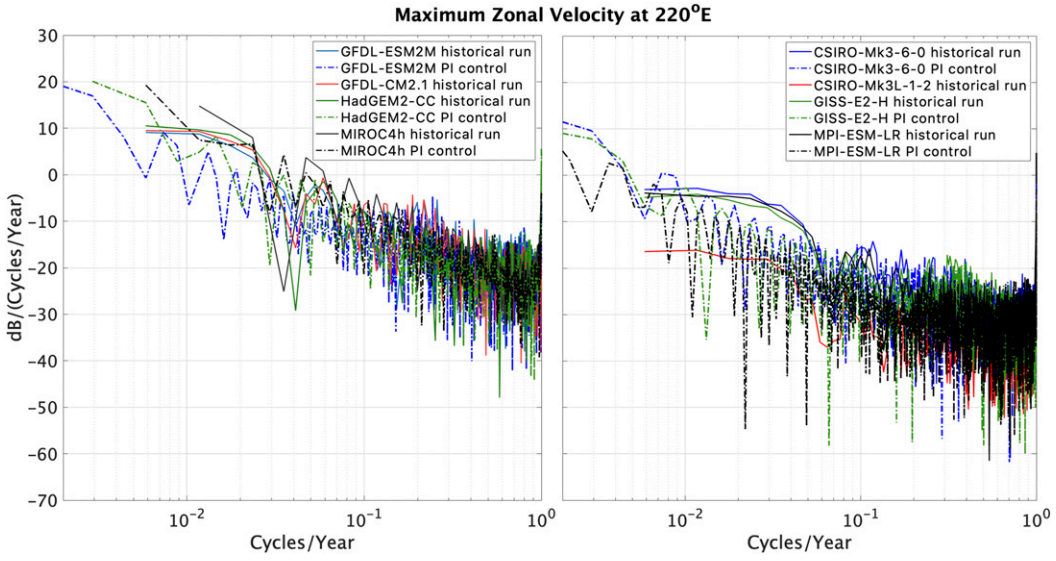

FIG. 5. Periodogram of maximum velocity in the EUC core at 220°E for the CMIP5 models with the best and poorest simulation of the undercurrent. A single historical run from each simulation is used (solid lines), and the preindustrial control run (dashed lines) is shown separately for those models that have one.

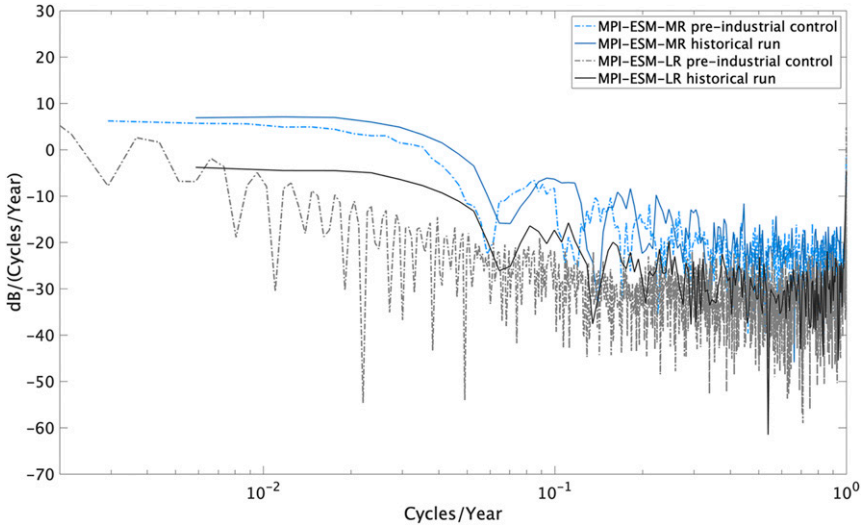

FIG. 6. Periodogram of maximum velocity in the EUC core at 220°E MPI-ESM at a low-resolution and mixed-resolution simulation.

and vertical gradients, especially in the eastern Pacific) may be important for improving model simulations of Pacific decadal variability. Comparisons of CMIP5 models with more realistic simulations of the EUC suggest that resolution as well as diffusivity and viscosity parameterizations are key to improvement in the simulation of the EUC.

Acknowledgments. We thank Henry Marshall for all his assistance with data wrangling and data visualization. We acknowledge the World Climate Research Programme's Working Group on Coupled Modelling, which is responsible for CMIP, and we thank the climate modeling groups (listed in Table 1 of this paper) for producing and making available their model output. For CMIP the U.S. Department of Energy's Program for Climate Model Diagnosis and Intercomparison provides coordinating support and led development of software infrastructure in partnership with the Global Organization for Earth System Science Portals. This material is based upon work supported by a National Science Foundation Graduate Research Fellowship (Grant DGE1144152) to author Kuntz and a Star Family Challenge Grant to author Schrag.

Data Availability Statement. Data from the CMIP5 multimodel ensemble archive was provided by the Earth System Grid Federation (https://esgf.llnl.gov/). Data from the Tropical Atmosphere Ocean Project came from the TAO Project Office (2000) of NOAA/PMEL.

REFERENCES

Alexander, M. A., I. Blade, M. Newman, J. R. Lanzante, N.-C Lau, and J. D. Scott, 2002: The atmospheric bridge: The influence of ENSO teleconnections on air–sea interaction over the global oceans. *J. Climate*, **15**, 2205–2231, https://doi.org/10.1175/1520-0442(2002)015<2205:TABTIO>2.0.CO;2.

Bellenger, H., E. Guilyardi, J. Leloup, M. Lengaigne, and J. Vialard, 2014: ENSO representation in climate models: From CMIP3 to CMIP5. *Climate Dyn.*, **42**, 1999–2018, https://doi.org/10.1007/s00382-013-1783-z.

Bjerknes, J., 1966: A possible response of the atmospheric Hadley circulation to equatorial anomalies of ocean temperature. *Tellus*, **18**, 820–829, https://doi.org/10.3402/tellusa.v18i4.9712.

Broecker, W., 2017: When climate change predictions are right for the wrong reason. *Climatic Change*, **142**, 1–6, https://doi.org/10.1007/s10584-017-1927-y.

Brown, J. N., J. S. Godfrey, and S. E. Wijffels, 2010: Nonlinear effects of tropical instability waves on the equatorial Pacific circulation. *J. Phys. Oceanogr.*, **40**, 381–393, https://doi.org/10.1175/2009JPO3963.1.

Bryden, H. L., and E. C. Brady, 1985: Diagnostic model of the three-dimensional circulation in the upper equatorial Pacific Ocean. *J. Phys. Oceanogr.*, **15**, 1255–1273, https://doi.org/10.1175/1520-0485(1985)015<1255:DMOTTD>2.0.CO;2.

Burls, N. J., and A. V. Fedorov, 2014: What controls the mean east-west sea surface temperature gradient in the equatorial Pacific: The role of cloud albedo. *J. Climate*, **27**, 2757–2778, https://doi.org/10.1175/JCLI-D-13-00255.1.

Coats, S., and K. B. Karnauskas, 2018: A role for the Equatorial Undercurrent in the ocean dynamical thermostat. *J. Climate*, **31**, 6245–6261, https://doi.org/10.1175/JCLI-D-17-0513.1.

Collier, M., S. Jeffrey, L. Rotstayn, K. Wong, S. Dravitzki, C. Moeseneder, C. Hamalainen, and J. Syktus, 2011: The CSIRO-Mk3-6-0 atmosphere-ocean GCM: Participation in CMIP5 and data publication. *MODSIM11 Int. Congress on Modelling and Simulation*, Perth, WA, Modelling and Simulation Society of Australia and New Zealand, 2691–2697, http://hdl.handle.net/102.100.100/102077?index=1.

Dawson, A., A. J. Matthews, D. P. Stevens, M. J. Roberts, and P. L. Vidale, 2013: Importance of oceanic resolution and mean state on the extra-tropical response to El Niño in a matrix of coupled models. *Climate Dyn.*, **41**, 1439–1452, https://doi.org/10.1007/s00382-012-1518-6.

Drenkard, E. J., and K. B. Karnauskas, 2014: Strengthening of the Pacific Equatorial Undercurrent in the SODA reanalysis: Mechanisms, ocean dynamics, and implications. *J. Climate*, **27**, 2405–2416, https://doi.org/10.1175/JCLI-D-13-00359.1.

Dufresne, J.-L., and Coauthors, 2013: Climate change projections using the IPSL-CM5 Earth system model: From CMIP3 to CMIP5. *Climate Dyn.*, **40**, 2123–2165, https://doi.org/10.1007/s00382-012-1636-1.

Dunne, J. P., and Coauthors, 2012: GFDL's ESM2 global coupled climate–carbon Earth system models. Part I: Physical formulation and baseline simulation characteristics. *J. Climate*, **25**, 6646–6665, https://doi.org/10.1175/JCLI-D-11-00560.1.

England, M., and Coauthors, 2014: Recent intensification of wind-driven circulation in the Pacific and the ongoing warming hiatus. *Nat. Climate Change*, **4**, 222–227, https://doi.org/10.1038/nclimate2106.

Fyfe, J., and N. Gillett, 2014: Recent observed and simulated warming. *Nat. Climate Change*, **4**, 150–151, https://doi.org/10.1038/nclimate2111.

Gent, P. R., and J. C. McWilliams, 1990: Isopycnal mixing in ocean circulation models. *J. Phys. Oceanogr.*, **20**, 150–155, https://doi.org/10.1175/1520-0485(1990)0200150:IMIOCM2.0.CO;2.

——, J. Willebrand, T. J. McDougall, and J. C. McWilliams, 1995: Parameterizing eddy-induced tracer transports in ocean circulation models. *J. Phys. Oceanogr.*, **25**, 463–474, https://doi.org/10.1175/1520-0485(1995)025<0463:PEITTI>2.0.CO;2.

Gordon, H. B., S. P. O'Farrell, M. A. Collier, M. R. Dix, L. D. Rotstayn, E. A. Kowalczyk, A. C. Hirst, and I. G. Watterson, 2010: The CSIRO Mk3.5 climate model. CAWCR Tech. Rep. 021, 74 pp., http://hdl.handle.net/102.100.100/108810?index=1.

Griffies, S. M., and Coauthors, 2005: Formulation of an ocean model for global climate simulations. *Ocean Sci.*, **1**, 45–79, https://doi.org/10.5194/os-1-45-2005.

——, and Coauthors, 2011: The GFDL CM3 coupled climate model: Characteristics of the ocean and sea ice simulations. *J. Climate*, **24**, 3520–3544, https://doi.org/10.1175/2011JCLI3964.1.

Guilyardi, E., 2006: El Nino-mean state-seasonal cycle interactions in a multi-model ensemble. *Climate Dyn.*, **26**, 329–348, https://doi.org/10.1007/s00382-005-0084-6.

——, H. Bellenger, M. Collins, S. Ferrett, W. Cai, and A. Wittenberg, 2012: A first look at ENSO in CMIP5. *CLIVAR Exchanges*, No. 17, International CLIVAR Project Office, Southampton, United Kingdom, 29–32.

Haidvogel, D. B., and A. Beckmann, 1999: *Numerical Ocean Circulation Modeling*. Imperial College Press, 318 pp.

Imada, Y., and M. Kimoto, 2006: Improvement of thermocline structure that affect ENSO performance in a coupled GCM. *SOLA*, **2**, 164–167, https://doi.org/10.2151/SOLA.2006-042.

Jin, F.-F., S. T. Kim, and L. Bejarano, 2006: A coupled-stability index for ENSO. *Geophys. Res. Lett.*, **33**, L23708, https://doi.org/10.1029/2006GL027221.

Jochum, M., and R. Murtugudde, 2006: Temperature advection by tropical instability waves. *J. Phys. Oceanogr.*, **36**, 592–605, https://doi.org/10.1175/JPO2870.1.

——, G. Danabasoglu, M. Holland, Y. O. Kwon, and W. Large, 2008: Ocean viscosity and climate. *J. Geophys. Res.*, **113**, C06017, https://doi.org/10.1029/2007JC004515.

Johns, T. C., and Coauthors, 2006: The new Hadley Centre climate model HadGEM1: Evaluation of coupled simulations. *J. Climate*, **19**, 1327–1353, https://doi.org/10.1175/JCLI3712.1.

Jungclaus, J. H., and Coauthors, 2013: Characteristics of the ocean simulations in the Max Planck Institute Ocean Model (MPIOM) the ocean component of the MPI-Earth system model. *J. Adv. Model. Earth Syst.*, **5**, 422–446, https://doi.org/10.1002/jame.20023.

Karnauskas, K. B., R. Murtugudde, and A. J. Busalacchi, 2007: The effect of the Galápagos Islands on the equatorial Pacific cold tongue. *J. Phys. Oceanogr.*, **37**, 1266–1281, https://doi.org/10.1175/JPO3048.1.

——, ——, and ——, 2008: The effect of the Galápagos Islands on ENSO in forced ocean and hybrid coupled models. *J. Phys. Oceanogr.*, **38**, 2519–2534, https://doi.org/10.1175/2008JPO3848.1.

——, G. C. Johnson, and R. Murtugudde, 2012: An equatorial ocean bottleneck in global climate models. *J. Climate*, **25**, 343–349, https://doi.org/10.1175/JCLI-D-11-00059.1.

Kohyama, T., D. L. Hartmann, and D. S. Battisti, 2017: La Niña–like mean-state response to global warming and potential oceanic roles. *J. Climate*, **30**, 4207–4225, https://doi.org/10.1175/JCLI-D-16-0441.1.

Kosaka, Y., and S. Xie, 2013: Recent global-warming hiatus tied to equatorial Pacific surface cooling. *Nature*, **501**, 403–407, https://doi.org/10.1038/nature12534.

Kraus, E., and J. Turner, 1967: A one-dimensional model of the seasonal thermocline. II: The general theory and its consequences. *Tellus*, **19**, 98–106, https://doi.org/10.3402/tellusa.v19i1.9753.

Kuntz, L. B., and D. P. Schrag, 2018: Hemispheric asymmetry in the ventilated thermocline of the tropical Pacific. *J. Climate*, **31**, 1281–1288, https://doi.org/10.1175/JCLI-D-17-0686.1.

Large, W. G., J. C. McWilliams, and S. C. Doney, 1994: Oceanic vertical mixing: A review and a model with a nonlocal boundary layer parameterization. *Rev. Geophys.*, **32**, 363–403, https://doi.org/10.1029/94RG01872.

Li, G., Y. Du, H. Xu, and B. Ren, 2015: An intermodel approach to identify the source of excessive equatorial Pacific cold tongue in CMIP5 models and uncertainty in observational datasets. *J. Climate*, **28**, 7630–7640, https://doi.org/10.1175/JCLI-D-15-0168.1.

Lin, J., 2007: The double-ITCZ problem in IPCC AR4 coupled GCMs: Ocean–atmosphere feedback analysis. *J. Climate*, **20**, 4497–4525, https://doi.org/10.1175/JCLI4272.1.

Liu, C., A. Köhl, Z. Liu, F. Wang, and D. Stammer, 2016: Deep-reaching thermocline mixing in the equatorial pacific cold tongue. *Nat. Commun.*, **7**, 11576, https://doi.org/10.1038/ncomms11576.

Lyu, K., X. Zhang, J. A. Church, and J. Hu, 2016: Evaluation of the interdecadal variability of sea surface temperature and sea level in the Pacific in CMIP3 and CMIP5 models. *Int. J. Climatol.*, **36**, 3723–3740, https://doi.org/10.1002/joc.4587.

Martin, G. M., and Coauthors, 2011: The HadGEM2 family of Met Office Unified Model climate configurations. *Geosci. Model Dev.*, **4**, 723–757, https://doi.org/10.5194/gmd-4-723-2011.

Menkes, C. E., J. G. Vialard, S. C. Kennan, J. Boulanger, and G. V. Madec, 2006: A modeling study of the impact of tropical instability waves on the heat budget of the eastern equatorial Pacific. *J. Phys. Oceanogr.*, **36**, 847–865, https://doi.org/10.1175/JPO2904.1.

Mignot, J., D. Swingedouw, J. Deshayes, O. Marti, C. Talandier, R. Séférian, M. Lengaigne, and G. Madec, 2013: On the evolution of the oceanic component of the IPSL climate models from CMIP3 to CMIP5: A mean state comparison. *Ocean Modell.*, **72**, 167–184, https://doi.org/10.1016/j.ocemod.2013.09.001.

Moum, J. N., R.-C. Lien, A. Perlin, J. D. Nash, M. C. Gregg, and P. J. Wiles, 2009: Sea surface cooling at the Equator by subsurface mixing in tropical instability waves. *Nat. Geosci.*, **2**, 761–765, https://doi.org/10.1038/ngeo657.

Noh, Y., and H. J. Kim, 1999: Simulations of temperature and turbulence structure of the oceanic boundary layer with the improved near-surface process. *J. Geophys. Res.*, **104**, 15 621–15 634, https://doi.org/10.1029/1999JC900068.

Peters, H., M. C. Gregg, and J. M. Toole, 1988: On the parameterization of equatorial turbulence. *J. Geophys. Res.*, **93**, 1199–1218, https://doi.org/10.1029/JC093iC02p01199.

Phipps, S. J., L. D. Rotstayn, H. B. Gordon, J. L. Roberts, A. C. Hirst, and W. F. Budd, 2011: The CSIRO Mk3L climate system model version 1.0 – Part 1: Description and evaluation. *Geosci. Model Dev.*, **4**, 483–509, https://doi.org/10.5194/gmd-4-483-2011.

Richter, I., 2015: Climate model biases in the eastern tropical oceans: Causes, impacts and ways forward. *Wiley Interdiscip. Rev.: Climate Change*, **6**, 345–358, https://doi.org/10.1002/wcc.338.

Roberts, M. J., and Coauthors, 2009: Impact of resolution on the tropical Pacific circulation in a matrix of coupled models. *J. Climate*, **22**, 2541–2556, https://doi.org/10.1175/2008JCLI2537.1.

Sakamoto, T. T., and Coauthors, 2012: MIROC4h—A new high-resolution atmosphere-ocean coupled general circulation model. *J. Meteor. Soc. Japan*, **90**, 325–359, https://doi.org/10.2151/jmsj.2012-301.

Schmidt, G. A., and Coauthors, 2014: Configuration and assessment of the GISS ModelE2 contributions to the CMIP5 archive. *J. Adv. Model. Earth Syst.*, **6**, 141–184, https://doi.org/10.1002/2013MS000265.

Sheffield, J., and Coauthors, 2013: North American climate in CMIP5 experiments. Part II: Evaluation of historical simulations of intraseasonal to decadal variability. *J. Climate*, **26**, 9247–9290, https://doi.org/10.1175/JCLI-D-12-00593.1.

Small, R. J., and Coauthors, 2014: A new synoptic scale resolving global climate simulation using the Community Earth System Model. *J. Adv. Model. Earth Syst.*, **6**, 1065–1094, https://doi.org/10.1002/2014MS000363.

Sun, C., W. D. Smyth, and J. N. Moum, 1998: Dynamic instability of stratified shear flow in the upper equatorial Pacific. *J. Geophys. Res.*, **103**, 10 323–10 337, https://doi.org/10.1029/98JC00191.

Sun, S., and R. Bleck, 2006: Multi-century simulations with the coupled GISS-HYCOM climate model: Control experiments. *Climate Dyn.*, **26**, 407–428, https://doi.org/10.1007/s00382-005-0091-7.

TAO Project Office, 2000: Tropical Atmosphere Ocean/Triangle Trans-Ocean Buoy Network. NOAA/PMEL, accessed 21 July 2016, https://www.pmel.noaa.gov/tao/drupal/disdel/.

Thomas, M. D., and A. V. Fedorov, 2017: The eastern subtropical Pacific origin of the equatorial cold bias in climate models: A Lagrangian perspective. *J. Climate*, **30**, 5885–5900, https://doi.org/10.1175/JCLI-D-16-0819.1.

Trenberth, K. E., J. M. Caron, D. P. Stepaniak, and S. Worley, 2002: Evolution of El Niño-Southern Oscillation and global atmospheric surface temperatures. *J. Geophys. Res.*, **107**, 4065, https://doi.org/10.1029/2000JD000298.

——, J. T. Fasullo, G. Branstator, and A. S. Phillips, 2014: Seasonal aspects of the recent pause in surface warming. *Nat. Climate Change*, **4**, 911–916, https://doi.org/10.1038/nclimate2341.

van Oldenborgh, G. J., S. Y. Philip, and M. Collins, 2005: El Niño in a changing climate: A multi-model study. *Ocean Sci.*, **1**, 81–95, https://doi.org/10.5194/os-1-81-2005.

Visbeck, M., J. Marshall, and T. Haine, 1997: Specification of eddy transfer coefficients in coarse-resolution ocean circulation models. *J. Phys. Oceanogr.*, **27**, 381–402, https://doi.org/10.1175/1520-0485(1997)027<0381:SOETCI>2.0.CO;2.

Wang, H., and Coauthors, 2014: How well do global climate models simulate the variability of Atlantic tropical cyclones associated with ENSO? *J. Climate*, **27**, 5673–5692, https://doi.org/10.1175/JCLI-D-13-00625.1.

Yang, C., B. S. Giese, and L. Wu, 2014: Ocean dynamics and tropical Pacific climate change in ocean reanalyses and coupled climate models. *J. Geophys. Res. Oceans*, **119**, 7066–7077, https://doi.org/10.1002/2014JC009979.

Yu, J.-Y., and W. T. Liu, 2003: A linear relationship between ENSO intensity and tropical instability wave activity in the eastern Pacific Ocean. *Geophys. Res. Lett.*, **30**, 1735, https://doi.org/10.1029/2003GL017176.

Zhang, D., and M. J. McPhaden, 2006: Decadal variability of the shallow Pacific meridional overturning circulation: Relation to tropical sea surface temperatures in observations and climate change models. *Ocean Modell.*, **15**, 250–273, https://doi.org/10.1016/j.ocemod.2005.12.005.

Zhu, Y. C., and R. H. Zhang, 2018: An Argo-derived background diffusivity parameterization for improved ocean simulations in the tropical Pacific. *Geophys. Res. Lett.*, **45**, 1509–1517, https://doi.org/10.1002/2017GL076269.

Zuidema, P., and Coauthors, 2016: Challenges and prospects for reducing coupled climate model SST biases in the eastern tropical Atlantic and Pacific oceans: The U.S. CLIVAR Eastern Tropical Oceans Synthesis Working Group. *Bull. Amer. Meteor. Soc.*, **97**, 2305–2328, https://doi.org/10.1175/BAMS-D-15-00274.1.